Spectrochimica Acta Part A: Molecular and Biomolecular Spectroscopy 280 (2022) 121561

Contents lists available at ScienceDirect

Spectrochimica Acta Part A:
Molecular and Biomolecular Spectroscopy

journal homepage: www.journals.elsevier.com/spectrochimica-acta-part-a-molecular-and-biomolecular-spectroscopy

A novel wavelength modulation spectroscopy gas sensing technique with an ultra-compressed wavelength scanning bandwidth

Fupeng Wang [a,b], Rui Liang [a], Qingsheng Xue [a,*], Qiang Wang [b], Jinghua Wu [a], Yaopeng Cheng [a], Jiachen Sun [c], Qian Li [a]

[a] College of Information Science and Engineering, Ocean University of China, Qingdao, China
[b] State Key Laboratory of Applied Optics, Changchun Institute of Optics, Fine Mechanics and Physics, Chinese Academy of Sciences Changchun, 130033, China
[c] School of Information Science and Engineering and Shandong Provincial Key Laboratory of Laser Technology and Application, Shandong University, Qingdao 266237, China

HIGHLIGHTS

- The wavelength scanning bandwidth is ultra-compressed in WMS method;
- The residual amplitude modulation effect is almost completely eliminated;
- The thermal stability of laser diode is improved in WMS system;
- A temperature controller with < 0.001 °C precision is developed.

GRAPHICAL ABSTRACT

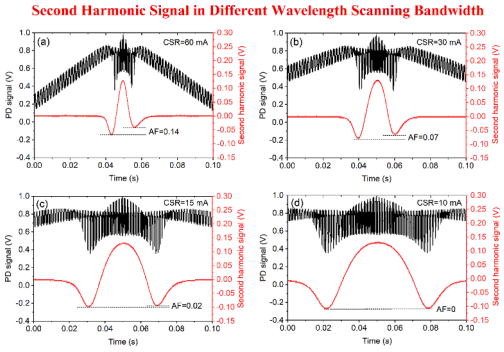

ARTICLE INFO

Keywords:
Wavelength modulation spectroscopy
Wavelength scanning bandwidth
Temperature control stability
Residual amplitude modulation

ABSTRACT

In a wavelength modulation spectroscopy (WMS) gas sensing system, a scanning ramp combined with a high frequency sinusoidal signal is applied to drive the laser source. Generally, a wide wavelength scanning bandwidth realized by voltage scanning ramp is required to fully cover the target gas absorption profile. In this paper, a novel WMS-based strategy is proposed and verified in a CH_4 detection system. The wavelength scanning bandwidth is compressed from ~659 pm to ~166 pm, even narrower than the half width at full height (HWFM) of the CH_4 absorption profile. In addition, the second harmonic signal that induced by the absorption is increased threefold by virtue of making full use of the dynamic range of the preamplifier circuit, and the waveform distortion that comes from the residual amplitude modulation (RAM) effect is eliminated as well. Benefiting from the compressed driving current range, the thermal stability of the laser diode is improved from the original level of 0.5 °C to 0.1 °C. As a result, a linear sensitivity of 75.2 ppb is achieved within 0–3000 ppm CH_4 concentration range at 12.7 s time constant.

* Corresponding author.
E-mail address: xueqingsheng@ouc.edu.cn (Q. Xue).

https://doi.org/10.1016/j.saa.2022.121561
Received 20 March 2022; Received in revised form 5 June 2022; Accepted 23 June 2022
Available online 27 June 2022

1. Introduction

Trace gas detection is widely used in many applications, for example the food & medicine safety, combustion analysis, environmental monitoring and industrial process control [1–6]. Various technologies have been developed for numerous kinds of gas detection, such as CH_4, C_2H_2, CO_2, CO, H_2S, etc. Nowadays, tunable diode laser absorption spectroscopy (TDLAS) has become the preferable option due to its unique advantages such as excellent selectivity, high sensitivity, robust anti-interference ability and long service life. According to the Beer-Lambert law, the detection sensitivity of the TDLAS system depends on the target gas absorption line strength and absorption path-length. So, in the simplest direct absorption spectroscopy (DAS) technique, the most straightforward way to enhance the detection sensitivity is extending the absorption path-length. Therefore, multi-pass cells including White cell and Herriott cell are designed, increasing the absorption path-length to tens of hundreds of meters level [7–9]. With the advent of this type of multi-pass cells, parts per billion (ppb) and sub-ppb level of minimum detection limit are achieved in CH_4 and C_2H_6 concentration detection. Another improvement approach is to select stronger absorption lines at mid-infrared (MIR) wavelength region instead of the commonly used near infrared (NIR) band. Therefore, MIR laser sources are gradually developed to exploit the strong fundamental rotation/vibration absorption lines considering that the absorption line strength of gas molecule in the MIR region is, in general, three orders of magnitude higher than the NIR band [10,11]. Recently, the rapid development of MIR tunable light source, such as inter-band cascade laser (ICL), quantum cascade laser (QCL), further reduced the cost and complexity of the MIR light source based TDLAS system compared to the past [12–16]. However, the need to actively cool both the lasers and detectors restricted the widespread use of such MIR systems. So, in order to achieve a high detection sensitivity and meanwhile avoid the limitations from MIR photoelectric detection, the WMS was subsequently proposed and immediately drawn dramatic attentions owing to its excellent noise rejection performance by virtue of the harmonic lock-in technique. In addition to the above-mentioned direct absorption technique, several indirect absorption spectroscopy (IDAS) techniques were successively proposed and advanced rapidly such as photoacoustic spectroscopy (PAS) [17–20], photothermal spectroscopy (PTS) [21] and light-induced thermoelastic spectroscopy (LITES) [22–24]. All these IDASs are zero-background techniques and a minimum detection limit (MDL) of parts per trillion (ppt) level has been realized in ultra-sensitive IDAS gas sensing system. However, these kinds of IDAS techniques, no matter PAS, PTS or LITES, are all based on the wavelength modulation-demodulation technique.

In a standard WMS-based gas sensing system, a low-frequency scanning ramp and a high-frequency sinusoidal signal are always combined to drive the laser source. Thus, both the output optical intensity and wavelength are modulated to interact with the target gas molecules. When configuring the driving parameters of laser source in WMS system, the sinusoidal signal amplitude is adjusted to meet the optimum wavelength modulation index of 2.2 to get the maximum second harmonic signal [25]. As to the low-frequency scanning ramp, sawtooth wave is usually chosen to realize a wide-band wavelength scanning, and the wavelength scanning bandwidth should be wide enough to cover a complete absorption profile. This indicates that the laser source operates under the driving current with a large scanning range. To our experience, the thermal stability of the laser will decrease if it undergoes a large driving current change compared with operating at a relatively constant current. Obviously, this would bring in negative influence on the gas detection sensitivity. In addition, it was reported that the nonlinearity wavelength response of the laser sources in WMS gas sensing system can introduce unexpected absorption-independent harmonics to the lock-in results [26]. Thus, an excessive wide wavelength scanning bandwidth will aggravate the influence from the nonlinearity response. In this study, we propose a novel strategy to upgrade the conventional WMS technique, by virtue of which the wavelength scanning bandwidth is substantially compressed. Meanwhile, the second harmonic amplitude is amplified, the influence of RAM is eliminated and the thermal stability of laser is improved as well. The afore-mentioned advantages are all of great benefit for the trace gas detection.

The rest of this study was organized as follows. Section 2 introduces the methodology of the ultra-compressed wavelength scanning bandwidth WMS technique. Section 3 demonstrates the experiment system and how the experiment conducted. Section 4 presents the experimental results and provides a brief comparison with the conventional WMS method. Finally, section 5 concludes this study.

2. Methodology

When laser output covers one or more absorption lines, the transmission of a probe light follows the absorption law of Beer-Lambert:

$$I(\nu) = I_0(\nu)\cdot exp[-\alpha(\nu)\cdot C\cdot L] \tag{1}$$

where $\alpha(\nu)$ is the absorption coefficient in unit of cm^{-1}, ν is the wave number, C is the concentration of sample gas, L is the absorption path-length, $I_0(\nu)$ is the intensity of incident light. In method of wavelength WMS system, we always combine a high frequency sinusoidal signal with a scanning ramp to drive a laser diode. The continuously frequency response and intensity response can be written as:

$$\nu = \vec{\nu} + \delta\nu\cdot\cos(\omega t) \tag{2}$$

$$I_0(\nu) = \vec{I}(\vec{\nu}) + \widetilde{I}(\vec{\nu}) + \Delta i\cdot\cos(\omega t + \varphi_1) + \Delta i_2\cdot\cos(2\omega t + \varphi_2) \tag{3}$$

where $\vec{\nu}$ is the slowly scanned optical frequency and $\delta\nu$ is the maximum excursions of ν around scanning wave number $\vec{\nu}$ (wavelength modulation depth), $\vec{I}(\vec{\nu})$ is the slowly scanned optical intensity which is linear response to $\vec{\nu}$ and $\widetilde{I}(\vec{\nu})$ is the residual from optical frequency-intensity nonlinearity, Δi is the linear optical intensity modulation depth and Δi_2 is the nonlinear optical intensity modulation depth, φ_1 and φ_2 are the phase shift between optical intensity and frequency modulation corresponding to the linear and nonlinear state respectively [2728]. Considering the approximation of $\alpha(\nu)\cdot C\cdot L << 1$ in the low concentration, the Eq. (1) and (3) can be re-expressed as:

$$I(\nu) = \vec{I}(\vec{\nu}) + \widetilde{I}(\vec{\nu}) + \Delta i\cdot\cos(\omega t + \varphi_1) + \underbrace{\Delta i_2\cdot\cos(2\omega t + \varphi_2)}_{p_1} - \underbrace{\vec{I}(\vec{\nu})\cdot[\alpha(\nu)\cdot C\cdot L]}_{p_2} - \underbrace{\widetilde{I}(\vec{\nu})\cdot[\alpha(\nu)\cdot C\cdot L]}_{p_3} - \underbrace{\Delta i\cdot\cos(\omega t + \varphi_1)\cdot[\alpha(\nu)\cdot C\cdot L]}_{p_4} - \underbrace{\Delta i_2\cdot\cos(2\omega t + \varphi_2)\cdot[\alpha(\nu)\cdot C\cdot L]}_{p_5} \tag{4}$$

The items p_1, p_2, p_3, p_4 and p_5 all contribute to the second harmonic signal, among which the item p_1 is absorption-independent and other items are absorption dependent. If applying a lock-in amplifier to measure the second harmonic of detected original signal, the result can be demonstrated as Eq. (5):

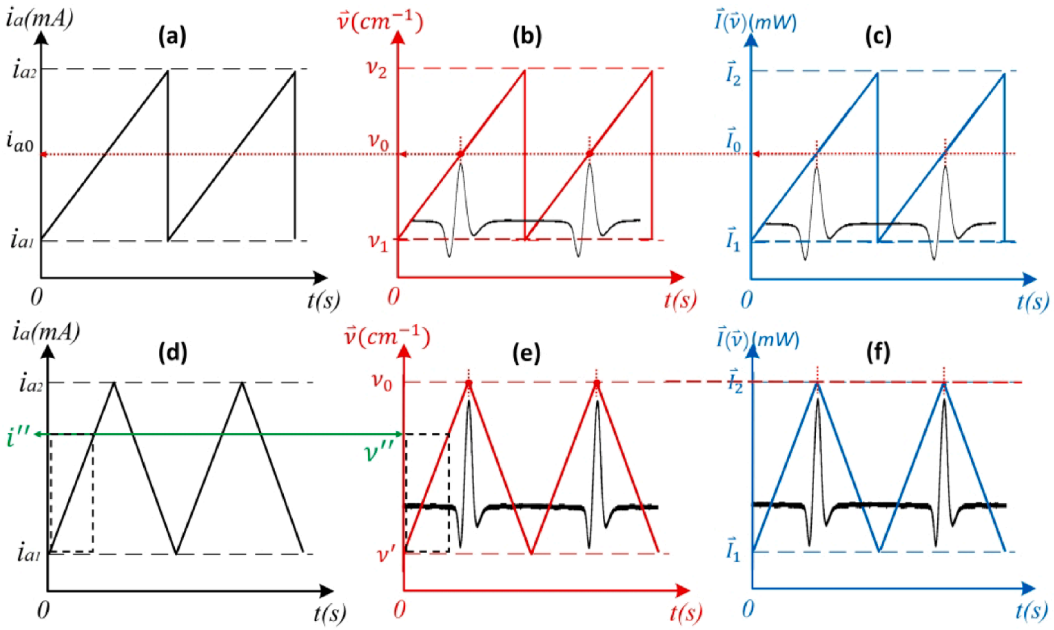

Fig. 1. (a, b, c) Principle example of conventional WMS technique utilizing a sawtooth scanning ramp. (d, e, f) Principle example of our proposed ultra-compressed WMS technique utilizing a triangular scanning ramp.

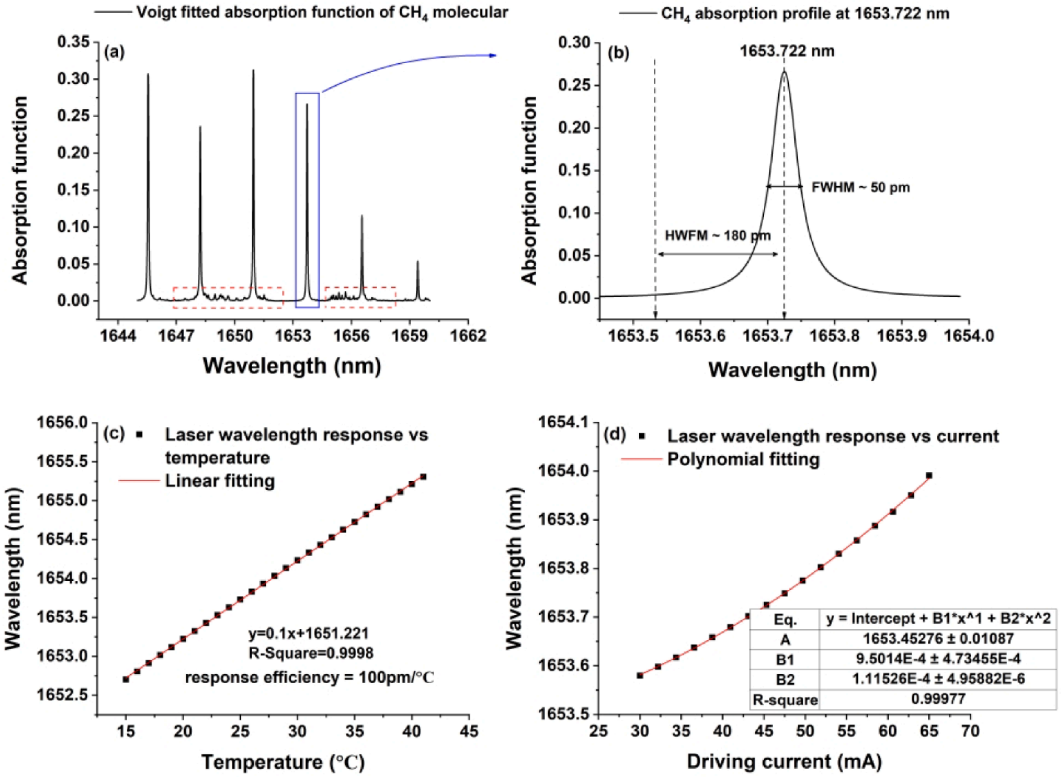

Fig. 2. (a) The absorption function of CH_4 simulated from 1645 nm to 1660 nm, (b) the absorption line shape of CH_4 at 1653.722 nm. (Simulation is performed at 296 K, 1 atm and 1 cm optical path length based on HITRAN2020 database) (c) The wavelength response towards internal temperature measured at 80 mA driving current, (d) The wavelength response towards driving current measured at 30 ℃ laser operating temperature.

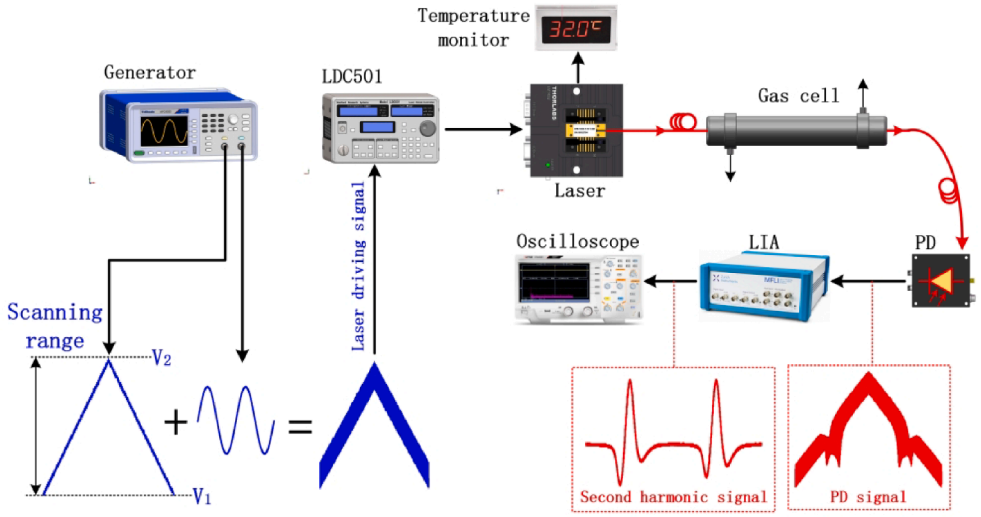

Fig. 3. Diagram of experiment system. PD: photodetector, LIA: lock-in amplifier.

$$S_{2nd} \propto \begin{cases} \underbrace{\Delta i_2 \cdot cos\Delta\phi_1}_{k_1} + \\ \underbrace{\vec{I}(\vec{\nu}) \cdot \alpha_0 \cdot \ C \cdot L \cdot a_2 \cdot cos\Delta\phi_2}_{k_2} + \\ \underbrace{\widetilde{I}(\vec{\nu}) \cdot \alpha_0 \cdot \ C \cdot L \cdot a_2 \cdot cos\Delta\phi_2}_{k_3} + \\ \underbrace{\Delta i \cdot \alpha_0 \cdot \ C \cdot L \cdot a_1 \cdot cos\Delta\phi_3 + \Delta i \cdot \alpha_0 \cdot \ C \cdot L \cdot a_3 \cdot cos\Delta\phi_4}_{k_4} + \\ \underbrace{\Delta i_2 \cdot \alpha_0 \cdot \ C \cdot L \cdot a_0 \cdot cos\Delta\phi_2}_{k_5} \end{cases} \tag{5}$$

α_0 represents the absorption coefficient at the absorption line center, a_0, a_1, a_2, a_3 are the zero, 1st, 2nd, 3rd items of Fourier expansion of $\alpha(\nu)$ in the case of Lorentzian profile, $\Delta\phi_1, \Delta\phi_2, \Delta\phi_3, \Delta\phi_4$ denote the phase differences between the lock-in reference and target signals [30]. In fact, item k_2 is the predominant 2nd harmonic component which we are interested to measure for concentration calculation. However, k_1, k_3, k_5 in the Eq. (5) coming from the optical frequency-intensity nonlinearity and k_4 coming from the RAM effect would bring in interference on the 2nd harmonic detection. In practice, the optical intensity is almost in linear relationship with the laser driving current, however, the optical frequency (wavelength) is nonlinear with the laser driving current. As a result, this is reason why we give a nonlinear residual term $\widetilde{I}(\vec{\nu})$ between optical intensity and optical frequency. Even though, we still can appropriately adjust the current scanning range (CSR) to ensure that the gas absorption line is fully covered within the wavelength scanning bandwidth.

The conventional strategy of WMS is displayed in Fig. 1 (a, b, c). A laser source is stabilized at temperature of T_1, and the slow scanning ramp is realized by a sawtooth current from i_{a1} to i_{a2} as shown in Fig. 1 (a). The wavelength response is simulated in Fig. 1 (b), the gas absorption line center ν_0 could be fixed at the middle of wavelength scanning range ν_1 ν_2 by adjusting the CSR ($i_{a2} - i_{a1}$) and i_{a0}. To simplify the methodological demonstration, the optical frequency is regarded as linear response in Fig. 1. The corresponding optical intensity response is displayed in Fig. 1 (c) which can be measured by a photodetector. As a result, the second harmonic signal ought to be locked at the middle of the scanning ramp. Generally, the maximum output $\vec{I}_2$ is *trans*-impedance amplified to the near-saturation voltage to make the most of the dynamic range of detection circuit, thus the $\vec{I}_0$ in Fig. 1 (c) is enlarged to the half of the maximum value which is proportional to the second harmonic amplitude.

In this paper, we upgrade the conventional WMS by compressing the wavelength scanning range with several special approaches, called ultra-compressed wavelength scanned WMS technique. Fig. 1 (d, e, f) illustrates how the ultra-compressed WMS technique is carried out. Instead of using a sawtooth scanning wave, a triangular current i_{a1} i_{a2} is generated to perform the wavelength scanning. In the next step, the temperature of laser source is tuned down from T_1 to T_2. As a result, the wavelength response ν_0 moves from the middle position (Fig. 1b) to the "vertex" as depicted in Fig. 1 (e). A complete second harmonic signal can still be recovered, thanks to the symmetric characteristic of Lorentzian or Voigt absorption profile as drawn in Fig. 1 (e, f). A longer flat baseline is recorded at the non-absorption region compared to the conventional WMS strategy in Fig. 1 (a, b, c). So, the wavelength scanning bandwidth of ($\nu_0 - \nu'$) can be remarkably compressed to ($\nu_0 - \nu''$) by adjusting the CSR from ($i_{a2} - i_{a1}$) to ($i_{a2} - i''$) as marked in Fig. 1 (d, e). Furthermore, the second harmonic amplitude is amplified by 2 times since the absorption location is shifted from the middle of the scanning ramp to the top of it. In the case of Fig. 1 (c), the second harmonic detection only uses half of the *trans*-impedance amplifier's dynamic range. However, the dynamic range is totally utilized in the case of Fig. 1 (f). Benefiting from the compressed wavelength scanning range, the laser source can work in an ultra-compressed CSR which is beneficial to the improvement of the system stability. The new ultra-compressed WMS technique and its advantages will be verified in detail in Section 3 and Section 4.

3. Experimental setup

Methane is chosen in experiment to validate the performance of the novel ultra-compressed WMS technique proposed in this study. To select an appropriate absorption line for the methane detection, the absorption spectrum from 1645 nm to 1660 nm is examined as plotted in Fig. 2 (a). Given that there is overmuch weak absorption interference around 1648.2 nm, 1650.9 nm and 1656.5 nm, we select 1653.7 nm as the target absorption line to measure the methane. The absorption line strength is $1.45 \times 10^{-21} cm/mol$ and the full width at half height (FWHM) as well as half width at full height (HWFM) are calculated to be 50pm and 180pm respectively as labelled in Fig. 2 (b). Since the target absorption line is determined, a distributed feedback (DFB) semiconductor laser operating at 1653 nm region is employed in the experiment system. The wavelength response is tested in advance as shown in Fig. 2 (c-d). The wavelength-temperature response efficiency is measured to be 100pm/°C as shown in Fig. 2 (c), as to the wavelength-current response efficiency, a polynomial fitting is performed and the

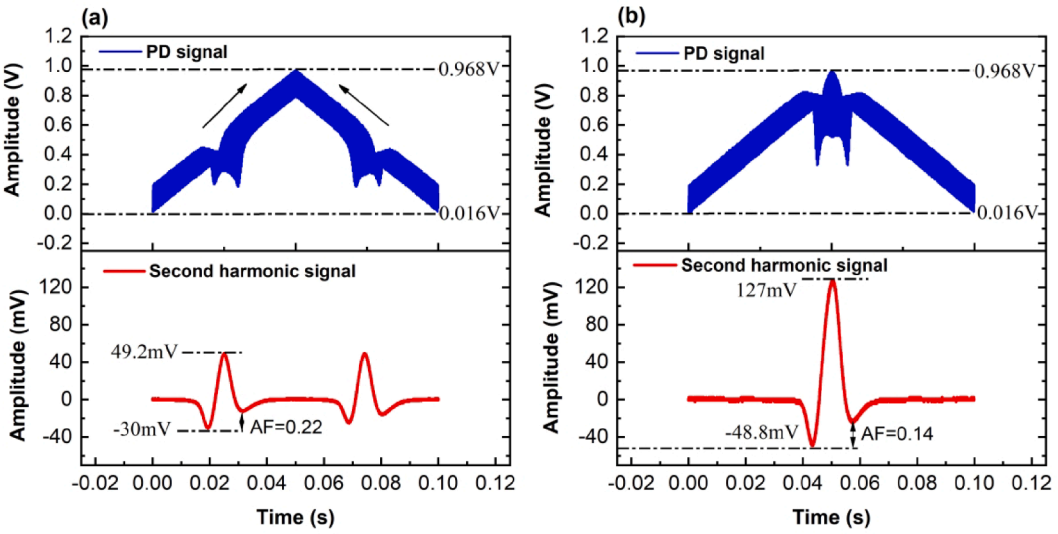

Fig. 4. (a) The photodetected original signal and the demodulated second harmonic signal from conventional WMS method, (b) the photodetected original signal and the demodulated second harmonic signal from ultra-narrow wavelength scanning bandwidth WMS method.

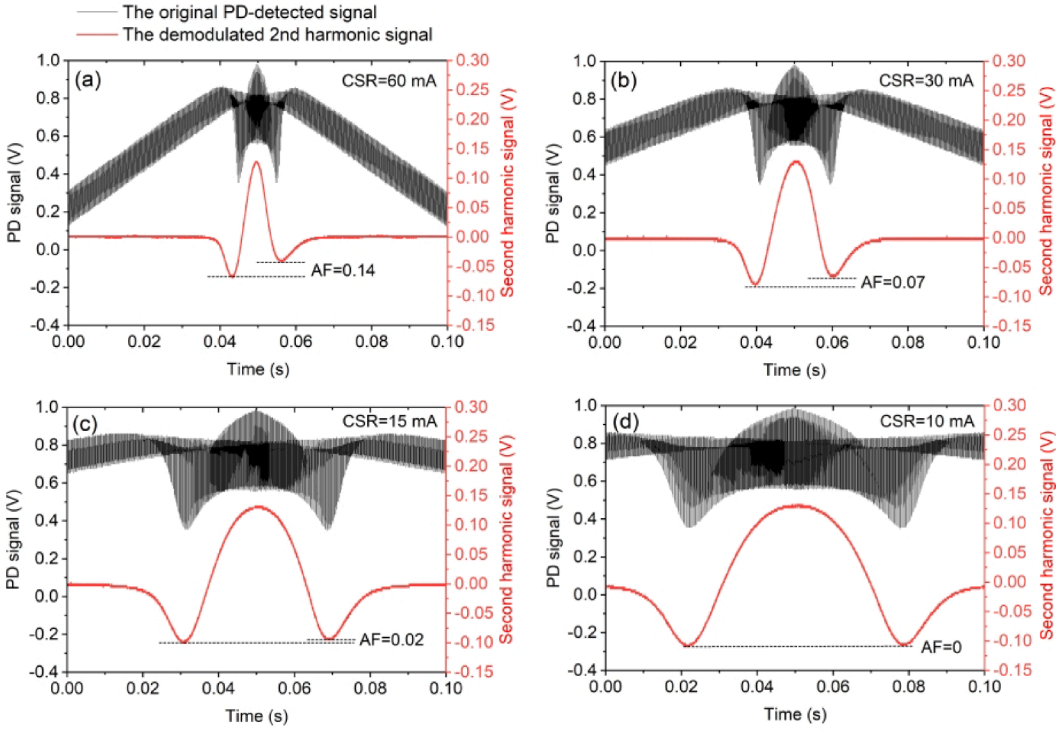

Fig. 5. The photodetected original signal and corresponding second harmonic signal in different CSR conditions.

result is displayed in Fig. 2 (d).

As displayed in Fig. 3, an experiment system is built up to validate the new method discussed in Section 2. A generator (AFG2000, Tektronix, USA) is used to provide a 10 Hz triangular wave for wavelength scanning and a 4 kHz, p-p 0.4 V sinusoidal signal for wavelength modulation. The triangular wave and sinusoidal signal are combined with a home-made adder circuit to drive the laser diode (DFB-1653-N-SM, Wuhan 69 Sensing Tech, CN) via a controller (LDC501, Stanford Research Systems, USA). The operating temperature of the laser diode is controlled by the LDC501 in the experiment section 4.1, 4.2 and 4.4. However, in the experiment section 4.3, the operating temperature of laser diode is controlled and monitored by a home-made laser controller instead of the LDC501. Within the home-made laser controller, a high-performance PID circuit is designed to monitor the NTC thermistor inside the laser package and then drive the TEC for heating and cooling. The voltage of NTC thermistor is recorded to calculate the laser operating temperature, and we use the temperature to indicate the thermal stability of laser diode in the following study. The temperature controlling performance of our home-made controller is tested with an ultra-high precision of < 0.001 °C, more information about our home-made laser controller is provided in the appendix. The laser output beam couples into a 3 m gas cell for absorption and the transmitted optical power is converted into voltage signal by a fiber-coupled photodetector (LSIPD-LD50-B-SMFA, Beijing Lightsensing

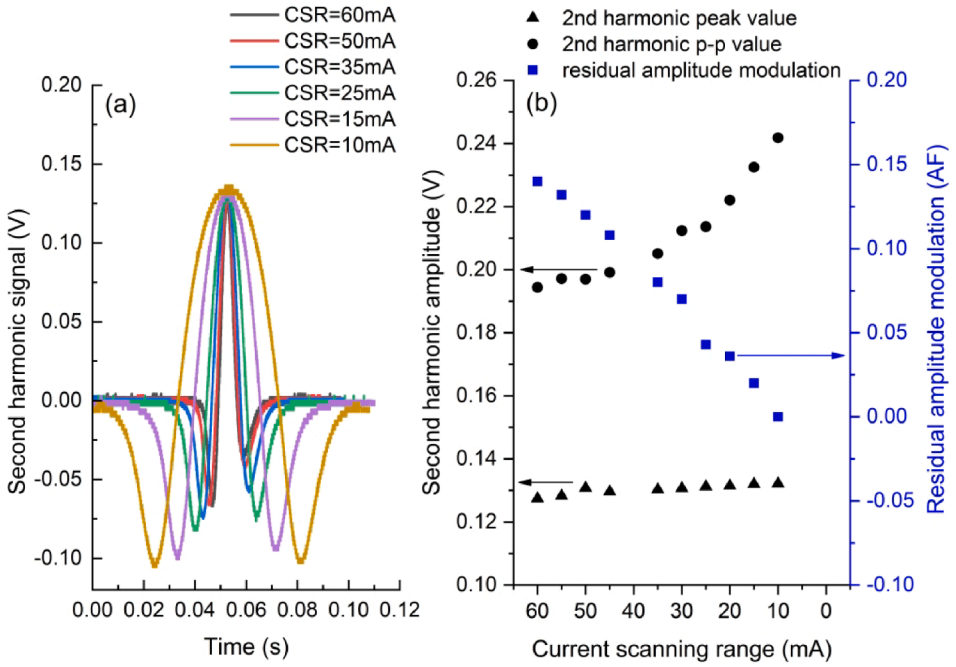

Fig. 6. (a) Second harmonic waves in different CSR of 60 mA, 50 mA, 35 mA, 25 mA, 15 mA and 10 mA, corresponding to different wavelength scanning bandwidths of 659 pm, 605 pm, 482 pm, 375 pm, 240 pm and 166 pm. (b) The relationship between second harmonic peak value (I_{max}), p-p value ($I_{max} - I_{min}$), RAM effect (AF in Eq. (6)) and different CSR.

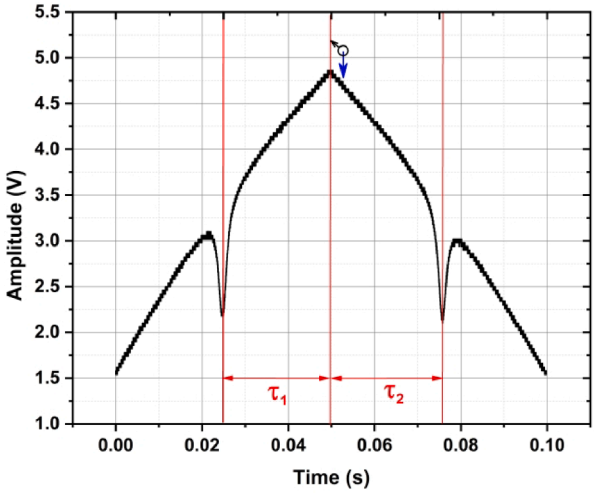

Fig. 7. Optical frequency-intensity phase difference observed in a single scanning recycle from direct absorption spectroscopy.

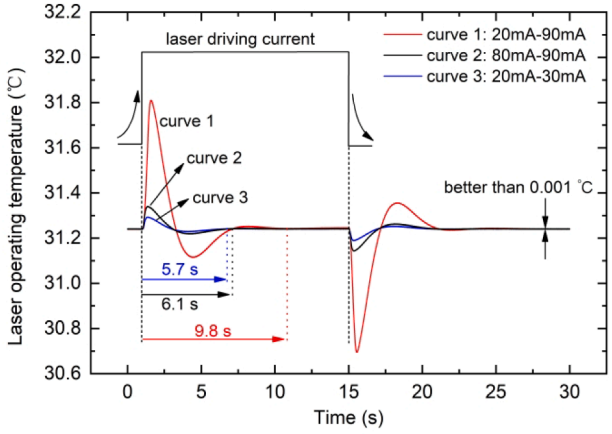

Fig. 8. Test of DFB laser operating temperature response when suddenly change its driving current.

Technologies Ltd, CN). The second harmonic signal is extracted by a lock-in amplifier (MFLI, Zurich Instruments, Zurich), and recorded with an oscilloscope (DPO3000, Tektronix, USA). Based on the experiment setup, we can easily adjust the CSR by changing the voltages V_1 and V_2 to control the laser wavelength scanning bandwidth. In addition, the operation temperature of DFB laser can be tuned by the LDC501, as a result, the central wavelength of scanning bandwidth can move back and forth in a bid to be aligned with the target gas absorption line. The CH_4 sample used in this study is provided by a gas mixing system as constructed in reference [29], including a customized mixing chamber, two flowmeters, 99.999% pure nitrogen and 1% methane.

4. Experimental results

In the experiments, we switch the WMS system from the conventional strategy to the newly proposed ultra-compressed wavelength scanned one. System performance parameters such as second harmonic amplitude, RAM effect and thermal stability of laser diode are evaluated and compared. The detailed procedures to compress the wavelength scanning bandwidth are introduced in Section 4.2, during which the thermal stability of laser diode is analyzed in Section 4.3. In the end, the gas detection performance of the upgraded WMS method is assessed through a CH_4 sensing experiment.

4.1. Realization of the ultra-compressed WMS technique

The voltages V_1 and V_2 of triangular wave, as labelled in Fig. 3, are set to be 0.4 V and 2.8 V respectively, corresponding to a CSR of 60 mA in the LDC501 controller with a 25 mA/V conversion rate. Considering

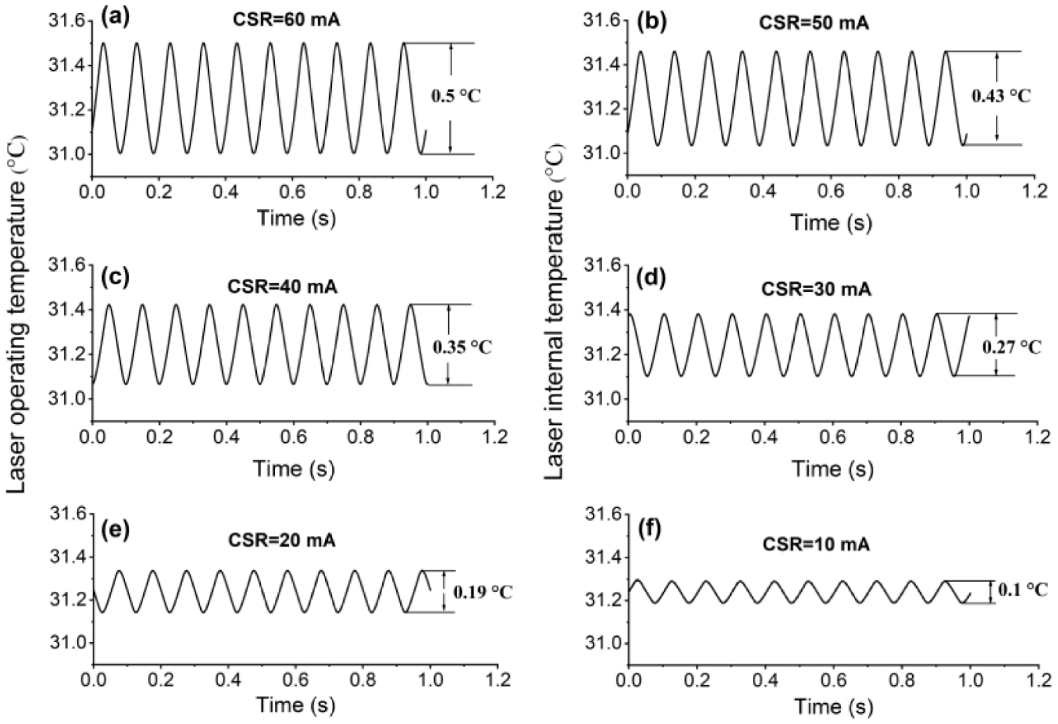

Fig. 9. The thermal stability of DFB laser when operating in different current scanning ranges.

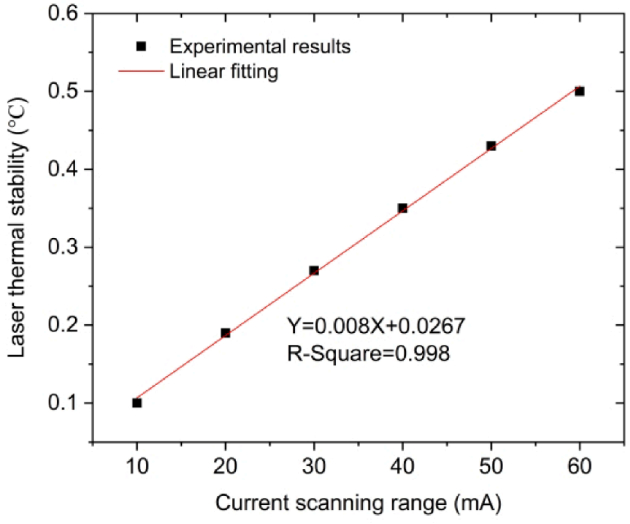

Fig. 10. The linear relationship between the DFB laser thermal stability and its current scanning range.

the 5 mA current modulation depth from p-p 0.4 V sinusoidal modulation signal, an offset current of 5 mA is provided by the LDC501 to make sure that the laser diode can always operate above the threshold current. Thus, a wavelength scanning bandwidth of 659 pm is realized according to the nonlinear results in Fig. 2 (d), which is wide enough to cover the complete absorption profile of CH_4 molecule. In the very beginning, the DFB laser operates at temperature of 29.2°C so that the CH_4 1653.7 nm absorption line is situated at the middle of the scanning ramp approximately as shown in Fig. 4 (a). In such a circumstance, two second harmonic signals are detected on the rising and falling ramps of triangular scanning respectively. To realize the ultra-compressed wavelength scanned WMS method, the laser operating temperature is lowered step by step to 25.75°C until two second harmonic signals meet at "vertex" of

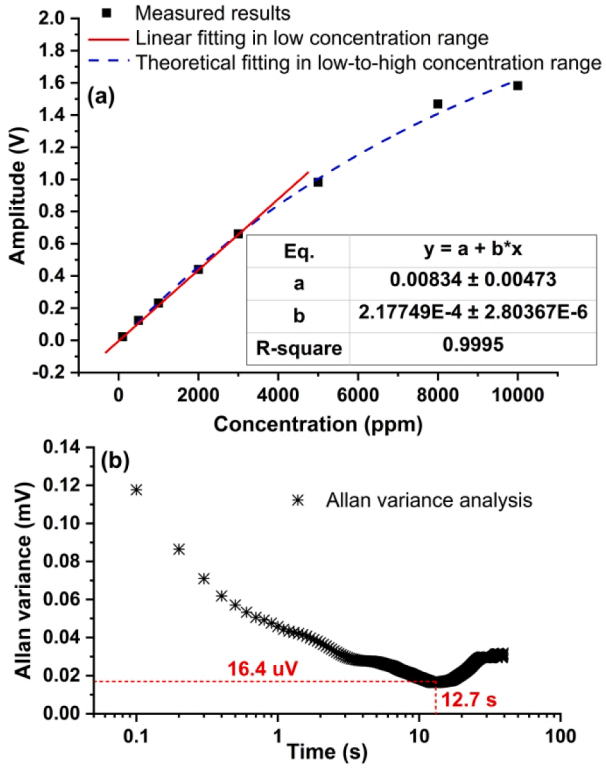

Fig. 11. Concentration detection experiment based on optimized ultra-compressed wavelength scanning bandwidth WMS method. (a) Linearity measurement in different methane concentrations from 100 ppm to 10000 ppm, (b) Allan variance analysis performed on the 1000 ppm results.

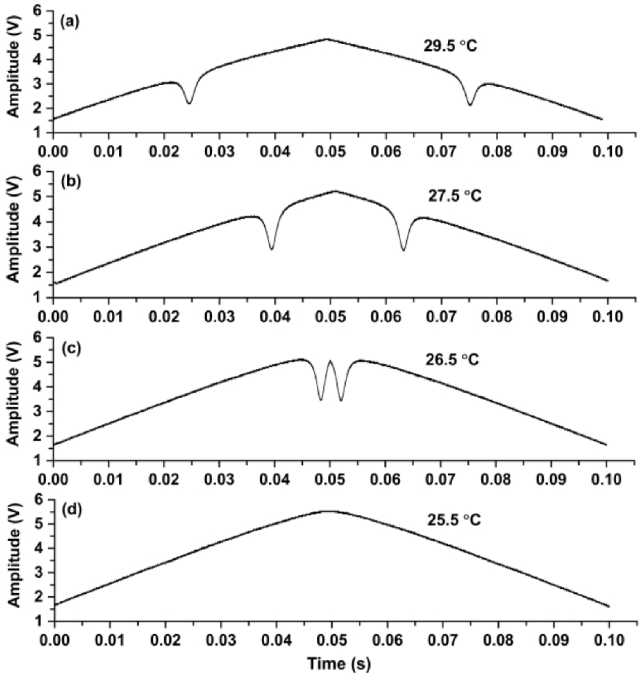

Fig. A1. A rough adjustment of laser operating temperature to find the approximate range.

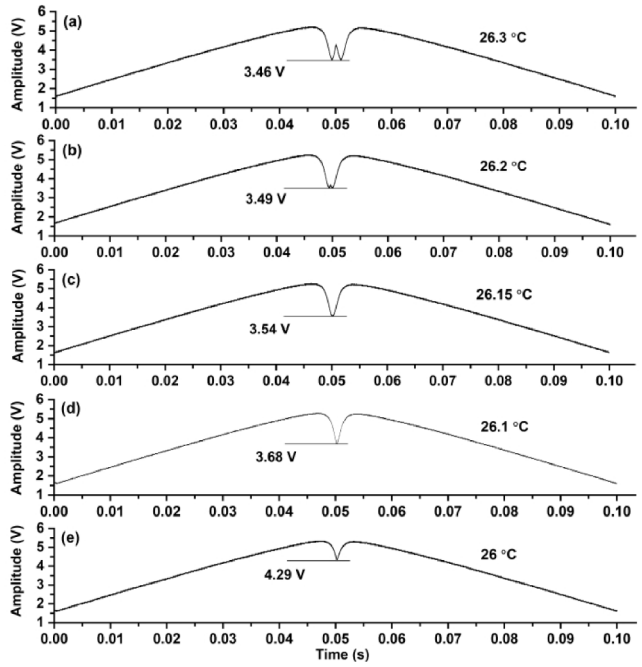

Fig. A2. A fine adjustment of laser operating temperature to find the exact location.

the triangular. This indicates that the 1653.7 nm absorption line has been moved to the top area as illustrated in Fig. 1 (d, e, f). The detailed procedure and the corresponding absorption curves are explained and displayed in the appendix. As a result, only one second harmonic signal is detected within a single triangular cycle. Obviously, the second harmonic amplitude is amplified by the factor of two compared to the one in Fig. 4 (a). The gain factor depends on the ratio of $\vec{I}_2/\vec{I}_0$ as marked in Fig. 1. To evaluate the degree of second harmonic distortion caused by RAM effect, a concept called asymmetry factor (AF) is defined like

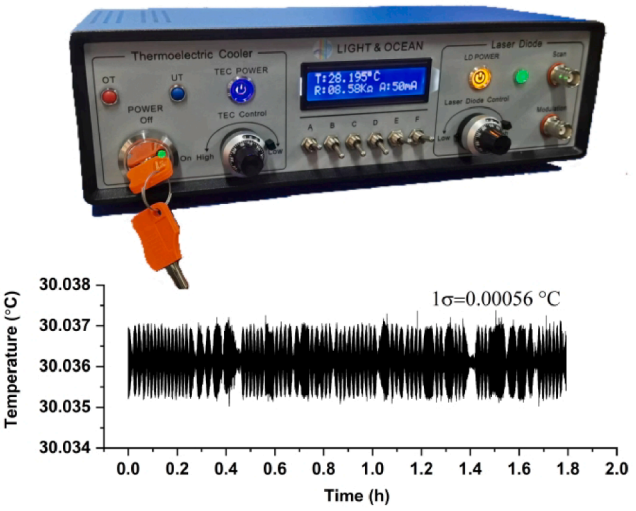

Fig. A3. Picture of our home-made laser controller and the tested temperature controlling precision.

references [3031].

$$AF = \frac{\Delta I_{min}}{I_{max} - I_{min}} \tag{6}$$

Where ΔI_{min} represents the difference of the two minima of the second harmonic signal, I_{max} represents maximum value of the second harmonic signal and I_{min} is the minimum value of the second harmonic signal. It is observed that the AF is slightly improved to 0.14 in ultra-compressed WMS method compared with the result of 0.22 in conventional WMS method. In the next section of 4.2, a detailed study will be performed to evaluate the improvement on second harmonic amplitude and RAM by gradually compressing the wavelength scanning bandwidth to ultimately realize the ultra-compressed WMS method.

4.2. *Steps to compress the wavelength scanning bandwidth*

After we have moved the CH_4 absorption line to the "vertex" of the triangular, there is only one second harmonic signal exists within a single scanning cycle, leading to surplus baseline recording in the non-absorption scanning region as depicted in Fig. 4 (b) and Fig. 5 (a) which is dispensable and unwanted. So, we increase the voltage of V_1 from the initial 0.4 V to 2.4 V and the CSR consequently decreases from 60 mA down to 10 mA. In the process, the wavelength scanning bandwidth is successfully compressed from 659 pm to 166 pm, and the photodetected signals together with demodulated second harmonic signal in several CSR conditions are recorded and displayed in Fig. 5 as below.

It is clear in Fig. 5 that the non-absorption baseline is getting shortened as the wavelength scanning bandwidth is compressed. Furthermore, the influence of RAM is thoroughly eliminated when the CSR is set to the value of 10 mA. During the process of compressing the CSR, we record all the second harmonic signals on the same chart as depicted in Fig. 6 (a), the amplitude variation that occurred during the process of wavelength scanning bandwidth compressing become manifest. The maximum values of second harmonic signals increase slowly while the minimum values keep decreasing as the CSR diminishes. As a result, a slowly rising curve and a surging curve are plotted in Fig. 6 (b), respectively showing the changes of the second harmonic signal's peak value and p-p value in the function of the CSR. In terms of the results presented in Fig. 6 (b), we reach the conclusion that smaller CSR is preferred to enhance the second harmonic amplitude and eliminate the RAM effect. However, it will become difficult to extract the non-absorption baseline if the wavelength scanning bandwidth is over

compressed. In this study, we set the wavelength scanning range compressed criterion as that when the RAM effect disappears as shown in Fig. 5 (d), then the corresponding parameters are determined. Of course, the CSR should be set $>$ 10 mA if we want to retain enough baseline in order to perform a better theoretical curve fitting. Moreover, in the situation where the gas concentration is the only concerned target, we can use the second harmonic $I_{max} - I_{min}$ to extrapolate the concentration, and then the CSR can be further compressed$<$10 mA as long as the I_{max} and I_{min} can be detected. It suggests that wavelength scanning bandwidth can be compressed narrower than HWFM in our WMS strategy without compromising the sensitivity of gas detection, which has never been reported before. Compared with the result in Fig. 4 (a), the second harmonic p-p value is amplified from 0.08 V to 0.24 V in total when we compress the CSR to 10 mA.

It is observed in Fig. 6 (a) that the I_{min} value of the second harmonic signal decreases as the CSR is compressed, the reason is easy to understand that the second harmonic is broadening. The principle is kind of similar with the phenomenon that the second harmonic curve would be broaden when increasing the modulation index in WMS system, and it has been observed in many published studies [32]. However, the I_{max} value also increases when we compress the CSR which is confusing. As we mentioned above, the CH_4 absorption line center is moved to the "vertex" of the triangular scanning wave, then the maximum value I_{max} should only depend on the optical intensity at "vertex" location and CH_4 absorption. As a result, the I_{max} value should not increase. We repeat our experiment and find two reasons to explain this phenomenon: The 1st reason is the low-pass filter of the lock-in amplifier. As we know there are high-frequency components located at amplitude mutation region of second harmonic. So, if the amplitude mutation gets smooth as compressing the CSR displayed in Fig. 6 (a), the amplitude-rejection effect would be weaken. As a result, the second harmonic amplitude gets increased. The 2nd reason comes from the optical frequency-intensity phase difference of laser diode as shown in Fig. 7. In practice, the absorption curves are not symmetrically distributed on the rising and falling sides of triangular scanning ramp strictly, which means the distance τ_2 is larger than τ_1 in Fig. 7. So, when we tune down the operating temperature as mentioned in section 4.1, two absorption curves would meet at blue-arrow position instead of the expected "vertex" point. In addition, it has been observed in our experiments that the blue-arrow position would move to the "vertex" as we compressing the CSR. This is a very interesting conclusion has not been reported before that the optical frequency-intensity phase difference not only relates to the scanning frequency [33] but also the scanning range. So, we should ceaselessly tune the operating temperature during compressing wavelength scanning range to adapt the change from optical frequency-intensity phase difference. In the end, the blue-arrow would nearly arrive at the "vertex" point. In the process, slight increase of I_{max} can be recorded as shown in Fig. 6 (a). Moreover, we believe this is also why the RAM effect disappears as compressing the wavelength scanning range, the symmetrical characteristic is getting better in the process. Of course, limitations still exist in the ultra-compressed WMS method. Even wavelength drift is not evaluated in this study. However, similar with the conventional WMS method, wavelength drift would also affect the second harmonic amplitude in the new ultra-compressed method. In this study, a scanning frequency of 10 Hz is used for the experimental verification. If the scanning frequency is increased, then the optical frequency-intensity phase difference would get larger considering the published results [33]. Afterwards, the operating temperature of laser diode should be adjusted to make sure two absorption curves overlap again as same with the above 2nd reason. In addition, pressure fluctuation will affect the ultimate wavelength compressed bandwidth due to the molecule's collision-induced broadening. So, the wavelength compressed parameters depend on the application environment.

4.3. Improvement on the thermal stability of DFB laser

Since the dynamic range of the laser's driving current is compressed substantially as discussed in section 4.2, an improved thermal stability should be expected inside the DFB laser for its workload is reduced. So, we carry out a simple experiment to study the temperature response during the sudden changes in the DFB laser's driving current as shown in Fig. 8. In the experiment of this section, the operating temperature of laser diode is controlled and monitored by our home-made laser controller instead of the LDC501. Within the home-made laser controller, PID temperature controlling module is activated to stabilize the operating temperature of DFB laser. The voltage of NTC thermistor is collected to calculate the laser operating temperature, and we use the calculated temperature to indicate the thermal stability of laser diode in this section. A square-wave current pulse is applied to drive the DFB laser, and simultaneously record its temperature response near the rising and falling edges. The steps of square-wave current are divided into three groups as 20–90 mA, 80–90 mA and 20–30 mA. It is easy to conclude that the larger switch of driving current will lead to more severe fluctuation of the laser temperature by comparing the monitored curve 1, curve 2 and curve 3, and will take more time to set down to a steady state. Furthermore, another conclusion can be drawn from the comparison between curve 2 and curve 3 that the DFB laser has proclivity to suffer a larger temperature fluctuation when operating in a high-current mode.

After the above experiment on the temperature response of the laser, the thermal stability of the laser diode is studied by compressing the CSR gradually from 60 mA down to 10 mA as depicted in Fig. 9. It should be noted that the laser temperature can be stabilized to an accuracy better than 0.001 °C when operating at constant current. However, unlike the static working mode, the operating temperature fluctuates periodically when the DFB laser is driven by a triangular wave scanning current. The thermal stability is defined as calculated and marked in Fig. 9, to evaluate the temperature fluctuation, and it is significantly improved with the compressing of the CSR. Furthermore, Fig. 10 is plotted to demonstrate the relationship between the laser thermal stability and the CSR. The linear fitting result reveals that the temperature vibration increases by 0.08 °C when the CSR rises by 10 mA. On the account of the process discussed in section 4.2 that the CSR is compressed from 60 mA to 10 mA, the thermal stability of laser temperature can thus be improved from 0.5 °C to 0.1 °C. This is of great help for improving the trace gas detection of TDLAS system because lower temperature fluctuation or higher temperature stability facilitates the reduction of the distortions in the measured absorption signals, which has been reported in our previous study [34].

4.4. Concentration measurement using new-proposed WMS method

In the last section of experiment, the concentration of CH_4 sample gas is controlled to vary from 100 ppm to 10000 ppm to test the new-proposed WMS method. The experimental parameters are optimized as: voltages V_1 and V_2 of triangular wave are set to the value of 2.4 V and 2.8 V respectively, corresponding to a CSR of 10 mA; the DFB laser operates at temperature of 25.75 $^{\circ}C$; the filter bandwidth of lock-in amplifier is set at $\sim$ 40 Hz. Nonlinearity is observed in high concentration range as depicted in Fig. 11 (a), which is consistent with the Beer-Lambert law simulated in blue dotted line. Linear fitting is performed within low concentration range from 100 ppm to 3000 ppm. As a result, an R-Square of 0.9995 is attained with an amplitude response of $218uV/ppm$. The noise level is studied by Allan variance analysis, which was performed at concentration of 1000 ppm. Because a 10 Hz triangular wave is used to realize the wavelength scanning, an effective value is calculated based on $I_{max} - I_{min}$ within 0.1 s. The Allan variance, including the background noise and the gas sensing uncertainty, show that a minimum noise of 16.4 uV is achieved at 12.7 s. Comparing the slope in Fig. 11 (a) and the minimum noise of 16.4 uV in Fig. 11 (b), a

minimum detection sensitivity of 75.2 ppb is realized at 12.7 s time constant within concentration range of 0–3000 ppm.

Here is a question that if we continue to decrease the CSR from 10 mA to zero, then the ultra-compressed wavelength scanning bandwidth WMS becomes the fixed-wavelength WMS method. This is an interesting point of view to analyze the advantages of the ultra-compressed WMS over conventional WMS, and further compare it with fixed-wavelength WMS method. Compared with the conventional WMS, the upgraded WMS method increases the second harmonic amplitude and improves the thermal stability of laser diode, which are beneficial for gas detection on sensitivity and stability. However, the low-pass filter bandwidth of lock-in amplifier does not change during the CSR compressing because the filtering bandwidth depends on the wavelength scanning frequency. However, the filtering bandwidth can be greatly narrowed in the fixed-wavelength WMS strategy because DC signal is outputted from the lock-in amplifier instead of AC harmonic wave. As a result, the signal to noise ratio (SNR) can be improved significantly. Even though, other limitation arises, for example, the wavelength drift is a big challenge which can affect the long-term stability and measurement accuracy. Then, wavelength locking technology should be developed to deal with the problem of fixed-wavelength WMS system. So, it is easy to understand that the SNR related parameters of the proposed ultra-compressed WMS method are better than conventional WMS, but are not good as fixed-wavelength WMS. However, the wavelength scanning WMS has advantages on long-term stability over fixed one considering the factor of wavelength drift. Furthermore, detected harmonic waveform instead of DC value has more information in addition to the gas concentration, for example the gas pressure.

5. Conclusion

In this paper, the widely used WMS technique is further upgraded into an ultra-narrow wavelength scanning bandwidth version by compressing the laser's driving current with specific temperature controlling. The theoretical analysis of this new method is introduced and the feasibility has been verified by a series of experiments. In addition to the triangular scanning wave used in this paper, sinewave can also be applied to act as the scanning waveform. We conclude four main outstanding advantages of our new method: (i) The second harmonic amplitude is enhanced considerably because the new method opens up the possibility to make full use of the maximum photodetected optical signal and the saturated dynamic range of electronic circuits. Additionally, the second harmonic amplitude is further increased during the process of wavelength scanning bandwidth compressing. In total, the second harmonic p-p value is amplified by 3 times in this paper. (ii) In conventional WMS-based gas sensing system, wide wavelength scanning range is usually preferred to cover the complete absorption profile of target gas which means the laser source is prone to operate in a large current range. However, the wavelength scanning bandwidth is substantially compressed in our method. Thus, the laser source is only required to work in a small dynamic range and we believe it is helpful to enhance its operating stability and service life. Although we simulate a linear wavelength response in Fig. 1 (b, e), in fact the nonlinearity of the wavelength response is always measurable as revealed in Fig. 2 (d). This kind of nonlinearity would introduce a series of absorption-independent harmonics to WMS sensing system as displayed in Eq. (5), disturbing the absorption dependent harmonic detection. Fortunately, the negative influence can be mitigated owing to the ultra-compressed wavelength scanning range. (iii) Waveform distortion that derives from the RAM effect can be eliminated in the new-proposed method. (iv) The thermal stability of the DFB laser becomes more stable in our new strategy, which is beneficial to improve the absorption detection. In addition, we believe this is helpful to extend the service life of laser sources as well. With the virtue of the afore-mentioned advantages, a linear sensitivity of 75.2 ppb is achieved within 0–3000 ppm concentration range in methane detection. As for its application, in our opinion, it is readily compatible with all the WMS-based gas sensing system including PAS, PTS and LITES systems since the method proposed in this paper is, in essence, an upgraded WMS technique.

CRediT authorship contribution statement

Fupeng Wang: Conceptualization, Methodology, Writing – original draft, Writing – review & editing. **Rui Liang:** Software, Validation, Investigation. **Qingsheng Xue:** Supervision, Project administration. **Qiang Wang:** Supervision. **Jinghua Wu:** Data curation, Visualization. **Yaopeng Cheng:** Writing – review & editing. **Jiachen Sun:** Formal analysis. **Qian Li:** Resources.

Declaration of Competing Interest

The authors declare that they have no known competing financial interests or personal relationships that could have appeared to influence the work reported in this paper.

Acknowledgement

National Natural Science Foundation of China (52001295, 62005267, 41575023, U2006209), Natural Science Foundation of Shandong Province (ZR2020QF097, ZR2021QD140), Open Fund of State Key Laboratory of Applied Optics (SKLAO2021001A12), Key Research and Development Program of Shandong Province (2020CXGC010706), Key project of major subject of new and old kinetic energy conversion in Shandong Province (2020XJDN010039), Fundamental Research Funds for the Central Universities (202013024, 202065004), Shandong Postdoctoral Innovation Program, National Key Research and Development Program of China (2019YFC1408301, 2018YFF01011003).

Appendix

1. *Detailed procedure of moving the absorption line center*

In this part, a direct wavelength scanning absorption spectroscopy (DAS) experiment is carried out to introduce the detailed procedure of moving the absorption line center to the top region of triangular wave. The reason of using DAS instead of WMS is that it is easier to observe the location of absorption curve in DAS signal. The first step is a rough adjustment as shown in Fig. A1. When tuning down the laser operating temperature by the LDC501, two absorption curves move towards the vertex of the triangular wave. After meeting at the top region, the absorption curve disappears like shown in Fig. A1(d). So, we can conclude that we should perform a fine adjustment of laser operating temperature between 26.5 °C and 25.5 °C to find the exact location where two absorption curves meet.

The second step is doing a fine adjustment with a temperature step of 0.1 °C as shown in Fig. A2. It is clear that two absorption curves have not met yet in Fig. A2 (a) and (b), however, the two absorption curves miss each in Fig. A2 (d) and (e) by comparing the labeled amplitudes 3.54 V, 3.68 V and 4.29 V in Fig. A2 (c, d, e). So, 26.15 °C is the exact operating temperature where two absorption curves overlap perfectly. Of course, a high-resolution ADC is helpful to improve the accuracy by adjusting the laser operating temperature per 0.01 °C step by step. It should be noted that the two absorption curves will separate again when compressing CSR due to the change of optical frequency-intensity phase difference as mentioned in section 4.2. So, the laser operating temperature of 26.15 °C should be re-adjusted repeating the above operation in the process of CSR compressing.

2. The home-made laser controller

Another laser temperature controlling function in addition the instrument LDC501 is provided by our home-made laser controller as shown in the picture of Fig. A3. The home-made laser controller has both functions of temperature controlling (left of the panel) and current driving (right of the panel). The current driving module provides three operating modes including constant current output, scanning current output and modulation current output. In this study, we only used the temperature controlling module. About the temperature controlling module, a high-performance PID circuit is designed to monitor the NTC thermistor and then drive the TEC for heating and cooling. The temperature controlling performance of our home-made controller is tested with an ultra-high precision < 0.001 °C as displayed in Fig. A3. In the experiment 4.3, the DFB laser pins of thermistor+, thermistor-, TEC + and TEC- are connected to our home-made laser controller. The high-level PID circuit is used to stabilize the laser operating temperature. Meanwhile, the voltage of thermistor is outputted on our circuit board, and collected by an ADC chip for temperature LCD display and data storage.

References

[1] P. Puligundla, J. Jung, S. Ko, Carbon dioxide sensors for intelligent food packaging applications, Food Control 25 (1) (2012) 328–333.
[2] M.E. Webber, J. Wang, S.T. Sanders, D.S. Baer, R.K. Hanson, In situ combustion measurements of CO, CO_2, H_2O and temperature using diode laser absorption sensors, Proc. Combust. Inst. 28 (1) (2000) 407–413.
[3] G. Wysocki, Y. Bakhirkin, S. So, F.K. Tittel, C.J. Hill, R.Q. Yang, M.P. Fraser, Dual interband cascade laser based trace-gas sensor for environmental monitoring, Appl. Opt. 46 (33) (2007) 8202–8210.
[4] F. Wang, J. Chang, X. Chen, Z. Wang, Q. Wang, Y. Wei, Z. Qin, Optical fiber oxygen sensor utilizing a robust phase demodulator, Measurement 95 (2017) 1–7.
[5] M. Righettoni, A. Amann, S.E. Pratsinis, Breath analysis by nanostructured metal oxides as chemo-resistive gas sensors, Mater. Today. 18 (3) (2015) 163–171.
[6] C. Wen, X. Huang, C. Shen, Multiple-pass enhanced Raman spectroscopy for fast industrial trace gas detection and process control, J. Raman Spectrosc. 51 (5) (2020) 781–787.
[7] K. Krzempek, M. Jahjah, R. Lewicki, P. Stefański, S. So, D. Thomazy, F.K. Tittel, CW DFB RT diode laser-based sensor for trace-gas detection of ethane using a novel compact multipass gas absorption cell, Appl. Phys. B 112 (2013) 461–465.
[8] W. Ren, W. Jiang, F.K. Tittel, Single-QCL-based absorption sensor for simultaneous trace-gas detection of CH4 and N2O, Appl. Phys. B 117 (2014) 245–251.
[9] K. Liu, L. Wang, T. Tan, G. Wang, W. Zhang, W. Chen, X. Gao, Highly sensitive detection of methane by near-infrared laser absorption spectroscopy using a compact dense-pattern multipass cell, Sens. Actuators B Chem. 220 (2015) 1000–1005.
[10] E.D. Hinkley, High–resolution infrared spectroscopy with a tunable diode laser, Appl. Phys. Lett. 16 (9) (1970) 351–354.
[11] J. Reid, B.K. Garside, J. Shewchun, M. El-Sherbiny, E.A. Ballik, High sensitivity point monitoring of atmospheric gases employing tunable diode lasers, Appl. Opt. 17 (11) (1978) 1806–1810.
[12] M. Horstjann, Y.A. Bakhirkin, A.A. Kosterev, R.F. Curl, F.K. Tittel, C.M. Wong, C. J. Hill, R.Q. Yang, Formaldehyde sensor using interband cascade laser based quartz-enhanced photoacoustic spectroscopy, Appl. Phys. B 79 (7) (2004) 799–803.
[13] R. Lewicki, G. Wysocki, A.A. Kosterev, F.K. Tittel, QEPAS based detection of broadband absorbing molecules using a widely tunable, cw quantum cascade laser at 8.4 μm, Opt. Express 15 (12) (2007) 7357–7366.
[14] V. Spagnolo, P. Patimisco, S. Borri, G. Scamarcio, B.E. Bernacki, J. Kriesel, Part-per-trillion level SF6 detection using a quartz enhanced photoacoustic spectroscopy-based sensor with single-mode fiber-coupled quantum cascade laser excitation, Opt. Lett. 37 (21) (2012) 4461–4463.
[15] L. Dong, R. Lewicki, K. Liu, P.R. Buerki, M.J. Weida, F.K. Tittel, Ultra-sensitive carbon monoxide detection by using EC-QCL based quartz-enhanced photoacoustic spectroscopy, Appl. Phys. B 107 (2) (2012) 275–283.
[16] Q. Ren, C. Chen, Y. Wang, C. Li, Y. Wang, A Prototype of ppbv-Level Midinfrared CO 2 Sensor for Potential Application in Deep-Sea Natural Gas Hydrate Exploration, IEEE Trans. Instrum. Measurement 69 (9) (2020) 7200–7208.
[17] Z. Lang, S. Qiao, Y. Ma, Acoustic microresonator based in-plane quartz-enhanced photoacoustic spectroscopy sensor with a line interaction mode, Opt. Lett. 47 (6) (2022) 1295–1298.
[18] X. Yin, L. Dong, H. Wu, H. Zheng, W. Ma, L. Zhang, W. Yin, S. Jia, F.K. Tittel, Sub-ppb nitrogen dioxide detection with a large linear dynamic range by use of a differential photoacoustic cell and a 3.5W blue multimode diode laser, Sens. Actuators B Chem. 247 (2017) 329–335.
[19] F. Wang, Q. Xue, J. Chang, Z. Wang, J. Sun, X. Luan, C. Li, Wavelength scanning Q-switched fiber-ring laser intra-cavity QEPAS using a standard 32.76 kHz quartz tuning fork for acetylene detection, Optics & Laser Technology 134 (2021), 106612.
[20] Y. Ma, Y. Hong, S. Qiao, Z. Lang, X. Liu, H-shaped acoustic micro-resonator-based quartz-enhanced photoacoustic spectroscopy, Opt. Lett. 47 (3) (2022) 601.
[21] C. Yao, S. Gao, Y. Wang, W. Jin, W. Ren, Heterodyne interferometric photothermal spectroscopy for gas detection in a hollow-core fiber, Sens. Actuators B Chem. 346 (2021), 130528.
[22] X. Liu, S. Qiao, Y. Ma, Highly sensitive methane detection based on light-induced thermoelastic spectroscopy with a 2.33 μm diode laser and adaptive Savitzky-Golay filtering, Opt. Express 30 (2) (2022) 1304.
[23] Y. Ma, Y. He, Y. Tong, X. Yu, F.K. Tittel, Quartz-tuning-fork enhanced photothermal spectroscopy for ultra-high sensitive trace gas detection, Opt. Express 26 (24) (2018) 32103–32110.
[24] X. Liu, Y. Ma, Sensitive carbon monoxide detection based on light-induced thermoelastic spectroscopy with a fiber-coupled multipass cell [Invited], Chin. Opt. Lett. 20 (2022), 031201.
[25] S. Schilt, L. Thevenaz, P. Robert, Wavelength modulation spectroscopy: combined frequency and intensity laser modulation, Appl. Opt. 42 (2003) 6728–6738.
[26] C. Zhu, P. Wang, T, F Peng, Y Sun, Second harmonic phase angle method based on WMS for background-free gas detection, IEEE Photonics Journal 13 (5) (2021) 1–6.
[27] K. Wang, M. Zhang, F. Duan, S. Xie, Y. Liao, Measurement of the phase shift between intensity and frequency modulations within DFB-LD and its influences on PGC demodulation in a fiber-optic sensor system, Appl. Opt. 52 (2013) 7194–7199.
[28] H. Li, G.B. Rieker, X. Liu, J.B. Jeffries, R.K. Hanson, Extension of wavelength-modulation spectroscopy to large modulation depth for diode laser absorption measurements in high-pressure gases, Appl. Opt. 45 (2006) 1052–1061.
[29] R. Liang, F. Wang, Q. Xue, Q. Wang, J. Wu, Y. Cheng, Q. Li, A Fourier-domain-based line shape recovery method used in direct absorption spectroscopy, Spectrochimica Acta Part A: Mol. & Biomol, Spectrosc. 275 (2022), 121153.
[30] F. Wang, J. Chang, Q. Wang, W. Wei, Z. Qin, TDLAS gas sensing system utilizing fiber reflector based round-trip structure: Double absorption path-length, residual amplitude modulation removal, Sens. Actuators A Phys. 259 (2017) 152–159.
[31] C. Zhu, J. Chang, P. Wang, W. Wei, Q. Wang, F. Wang, S. Zhang, Continuously wavelength-tunable light source with constant-power output for elimination of residual amplitude modulation, IEEE Sensors Journal 15 (1) (2015) 316–321.
[32] F. Wang, J. Chang, Q. Zhang, Z. Qin, C. Zhu, Pivotal techniques evaluation in QEPAS system for engineering applications, Measurement 135 (2019) 376–384.
[33] Y. Liu, J. Chang, J. Lian, Z. Liu, Q. Wang, C. Zhu, A time difference method for measurement of phase shift between distributed feedback laser diode (DFB-LD) output wavelength and intensity, Sensors 15 (2015) 16153–16161.
[34] Y. Xie, J. Chang, X. Chen, J. Sun, Q. Zhang, F. Wang, Z. Zhang, Y. Feng, A DFB-LD internal temperature fluctuation analysis in a TDLAS system for gas detection, IEEE Photonics J. 11 (2019) 6801708.